JACS
JOURNAL OF THE AMERICAN CHEMICAL SOCIETY
pubs.acs.org/JACS
Article

Following Nature's Footprint: Mimicking the High-Valent Heme-Oxo Mediated Indole Monooxygenation Reaction Landscape of Heme Enzymes

Pritam Mondal, Shanuk Rajapakse, and Gayan B. Wijeratne*

Cite This: https://doi.org/10.1021/jacs.1c11068
Read Online

ABSTRACT: Pathways for direct conversion of indoles to oxindoles have accumulated considerable interest in recent years due to their significance in the clear comprehension of various pathogenic processes in humans and the multipotent therapeutic value of oxindole pharmacophores. Heme enzymes are predominantly responsible for this conversion in biology and are thought to proceed with a compound-I active oxidant. These heme-enzyme-mediated indole monooxygenation pathways are rapidly emerging therapeutic targets; however, a clear mechanistic understanding is still lacking. Additionally, such knowledge holds promise in the rational design of highly specific indole monooxygenation synthetic protocols that are also cost-effective and environmentally benign. We herein report the first examples of synthetic compound-I and activated compound-II species that can effectively monooxygenate a diverse array of indoles with varied electronic and steric properties to exclusively produce the corresponding 2-oxindole products in good to excellent yields. Rigorous kinetic, thermodynamic, and mechanistic interrogations clearly illustrate an initial rate-limiting epoxidation step that takes place between the heme oxidant and indole substrate, and the resulting indole epoxide intermediate undergoes rearrangement driven by a 2,3-hydride shift on indole ring to ultimately produce 2-oxindole. The complete elucidation of the indole monooxygenation mechanism of these synthetic heme models will help reveal crucial insights into analogous biological systems, directly reinforcing drug design attempts targeting those heme enzymes. Moreover, these bioinspired model compounds are promising candidates for the future development of better synthetic protocols for the selective, efficient, and sustainable generation of 2-oxindole motifs, which are already known for a plethora of pharmacological benefits.

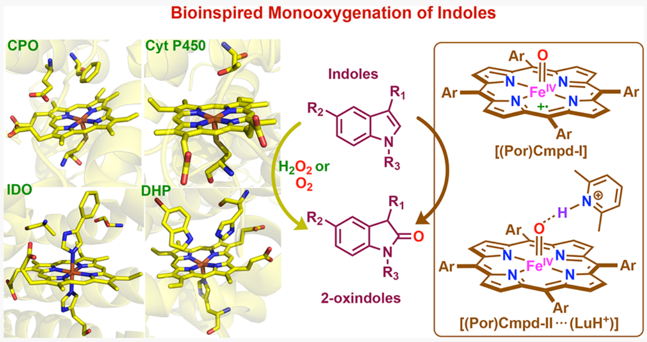

■ INTRODUCTION

Heme enzymes are powerhouses for a variety of pivotal transformations (e.g., oxidation, oxygenation, halogenation, nitration, nitrosation, dehydrogenation, epoxidation, etc.) involving biologically significant organic motifs, where oxygen (O_2)- and/or hydrogen peroxide (H_2O_2)-dependent active oxidants serve indispensable roles.[1−12] The vast heterogeneity of such reactivities constitute a rich knowledge base for the unequivocal comprehension of various physiological processes and their implications in pathogenesis and prognosis[13−19] while shedding light on how to maneuver enzymatic chemistries (or use their models) to successfully achieve synthetically complicated targets.[20−24] The efficient monooxygenation of indole moieties within biological systems is one such example, where heme enzymes are clearly the front-runners.[12] Chloroperoxidase (CPO),[25−27] dehaloperoxidase (DHP),[28,29] cytochrome P450 (Cyt P450),[30,31] horseradish peroxidase (HRP),[32] myoglobin (Mb),[33] indoleamine 2,3-dioxygenase (IDO),[34,35] and MarE,[36] a homologue of the tryptophan 2,3-dioxygenase (TDO) superfamily, have all been shown to mediate indole monooxygenation, albeit with varying efficacies and selectivities. In fact, a majority of these enzymes exhibit poor selectivities, often producing mixtures of 2- and 3-oxindoles upon indole oxygenation. CPO (Figure 1A) is undoubtedly the most superior in terms of selectivity and yield, and the corresponding oxygenation reaction proceeds via a H_2O_2-derived compound-I active oxidant (Figure 1C).[25] Intriguingly, DHP, Cyt P450, HRP, Mb, and IDO have all been proposed to oxygenate indoles via a similarly generated compound-I active species (Figure 1C),[28,30,32,34] and in contrast, DHP is the only heme enzyme that mediates the monooxygenation of (5-halo) indoles also via a putative

Received: October 19, 2021

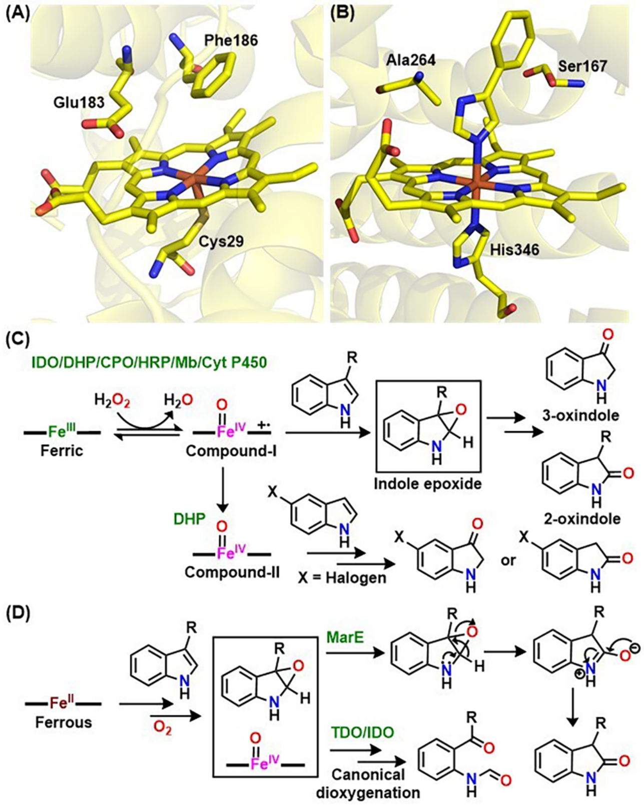

Figure 1. Crystallographically characterized active sites of (A) CPO (PDB: 1CPO[39]) and (B) human IDO (inhibitor bound; PDB: 2DOT[40]). (C) Proposed peroxygenase pathway for IDO/DHP/CPO/HRP/Mb/Cyt P450, where oxygenation of indole to the corresponding 2- and/or 3-oxindole is mediated by either a compound-I or compound-II intermediate. (D) Proposed mechanistic landscape for the monooxygenation of indole substrates by MarE and the canonical indole dioxygenation mediated by TDO/IDO enzymes; these exhibit bifurcated pathways with a common indole epoxide intermediate. In MarE, this intermediate has been proposed to rearrange via a 2,3-hydride shift to give the 2-oxindole product.

compound-II oxidant (Figure 1C);[28] compound-II is inferior to compound-I in its oxidizing capacities.[37,38]

Heme-enzyme-mediated indole monooxygenation pathways could have significant pathological implications, some of which, have already been highlighted in previous reports. Particularly, the products of lung Cyt P450-mediated oxygenation of 3-methylindole have been observed to exert pneumotoxic effects in mammals, although their roles have not yet been fully evaluated in humans.[41] Nonetheless, some reports suggest their involvement in lung cancer,[42,43] and thus, the successful inhibition of indole monooxygenation via Cyt P450 may possess some therapeutic value; noteworthily, future interrogations into such systems would greatly benefit from an unambiguous mechanistic understanding. Indole monooxygenating peroxygenase activity of IDO (Figure 1B) is another example of a pathogenically distinct pathway and is thought to be mechanistically parallel to the "peroxide shunt" of Cyt P450.[34] Importantly, this peroxygenase activity of IDO induces the effective inhibition of its native dioxygenase functionality. IDO and TDO have accumulated significant interest in recent years owing to their powerful therapeutic potential against a range of pathogenic conditions in humans, including an array of cancers.[44] Suitably, IDO/TDO inhibitors are rigorously sought after as therapeutic targets, especially in the design and development of immunotherapeutic anti-cancer agents.[15,45,46] Understanding the mechanistic specifics and precise structure−function relationships of the indole monooxygenation pathway of IDO therefore has definite therapeutic significance. Notably, such knowledge is also crucial for comprehending mechanism-based inhibition of IDO, where the effective quenching of its Fe(IV)-oxo reaction intermediate should, in theory, lead to oxindole products (Figure 1D, and see the mechanistic descriptions of MarE given below). Moreover, oxindoles themselves have been shown to effectively inhibit purified human IDO1, manifesting their promise as effective pharmacophores against cancer.[47] A member of the TDO superfamily, MarE, was recently shown to catalyze the conversion of 3-substituted indoles to 3-substituted-2-oxindoles under reducing conditions.[36] Importantly, MarE is the only heme enzyme that mediates indole monooxygenation utilizing $O_{2(g)}$ as the oxidant (Figure 1D). MarE follows a fascinating reaction landscape, in that it only inserts a single oxygen atom from dioxygen into the indole ring,[36] whereas in the canonical indole/tryptophan dioxygenation pathway (of IDO and TDO) both oxygen atoms are inserted into the indole 2,3-double bond leading to ring cleavage.[8,48−50] In MarE under reducing conditions, the dioxygenation pathway has been proposed to terminate midway due to the reduction of the ferryl intermediate, and the abandoned, unstable indole epoxide counterpart is thought to rearrange via a 2,3-hydride migration producing 2-oxindole products (Figure 1D).[36]

Intriguingly, the demand for highly efficient, sustainable methodologies for the generation of oxindoles have vertically advanced in the past two decades, mainly due to their versatile pharmacological properties. Oxindoles are privileged heterocyclic motifs that have emerged as key nuclei in a wide spectrum of bioactive alkaloids and pharmaceutically active compounds (Chart 1).[51−54] 2- and 3-oxindoles constitute this pivotal class of pharmacophores, and 2-oxindole and its derivatives have already been extensively incorporated in a wide variation of valuable building blocks for drug molecules with anti-cancer,[53,55] anti-tumor,[56] antioxidant,[57] anti-malarial,[58] anti-Alzheimer's,[59] hormone secretagogue,[60] antibacterial,[61] neuroprotective,[62] spermicidal,[63] anti-hypertension,[64] and analgesic applications;[65] 2-oxindole moieties are also found in the marketed anti-cancer drugs Sunitinib[66,67] and Palladia,[68] as well as in Indolidan[69] and Adibendan,[70] two superior therapeutic agents used to treat congestive heart failure (Chart 1). The pharmacological benefits of oxindole moieties are therefore just coming into light and are likely more multifaceted than currently known, underscoring a significant urgency for efficient, inexpensive, and sustainable synthetic protocols.

The likelihood of adapting the aforementioned indole monooxygenating heme enzymatic systems to address this need has been an interesting point of discussion in the contemporary literature; however, enzyme catalysis comes with its inherent drawbacks. When considering indole monooxygenation, those include (but are not limited to) (1) circumscribed substrate scopes with poor tolerance of functional groups and (2) tight restrictions in reaction conditions; in particular, the necessity for very low sample concentrations that are limited to aqueous media maintained within narrow pH windows (∼3−5) in order to prevent enzyme degradation. Rigorously designed bioinspired model systems can potentially circumvent most of these shortcomings, while serving as

https://doi.org/10.1021/jacs.1c11068
J. Am. Chem. Soc. XXXX, XXX, XXX−XXX

Chart 1. Examples of Natural Products and Chemically Synthesized Bioactive Compounds Containing 2-Oxindole Moieties (highlighted in green)

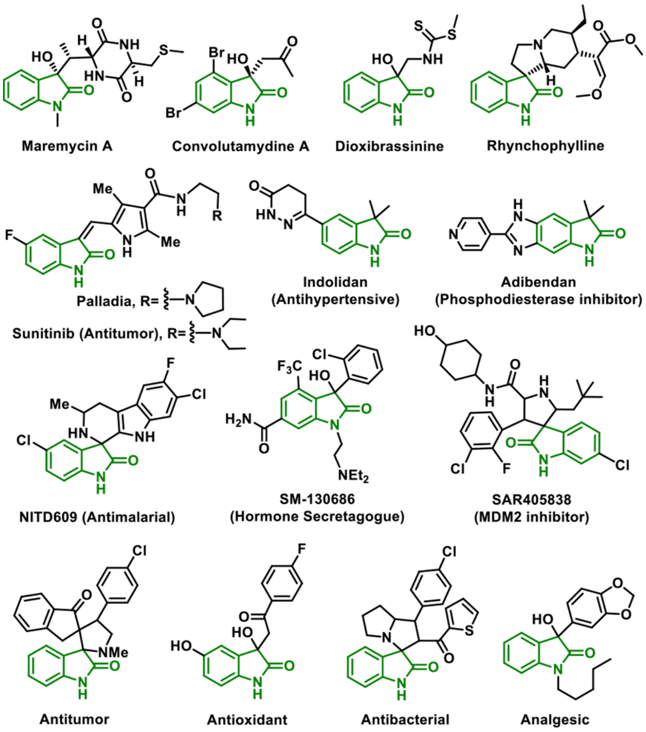

Scheme 1. Generalized Reaction Scheme Highlighting the Structural Variations of Heme Systems and Indole Substrates Involved in This Study[a]

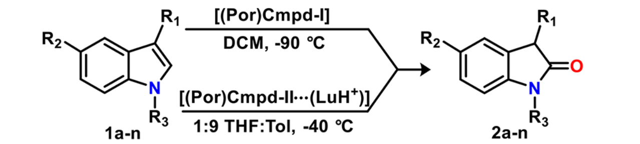

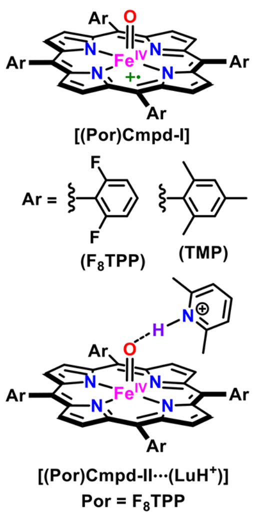

	R_1	R_2	R_3	Yield (%)
1a	H	H	H	80
1b	H	OMe	H	85
1c	H	Me	H	82
1d	H	Br	H	78
1e	H	CN	H	75
1f	H	H	Me	81
1g	Me	H	Me	80
1h	Me	H	H	88
1i	CH_2CN	H	H	85
1j	CH_2CO_2Et	H	H	80
1k	CH_2CH_2OH	H	H	78
1l	CH_2CH_2NHTs	H	H	75
1m	$CH_2CH_2NHCOCH_3$	OMe	H	72
1n	$CH_2CH(NHAc)-CO_2Me$	H	H	70

[a]All yields mentioned here have been obtained using [(F_8TPP)-Cmpd-I] as the oxidant.

powerful mechanistic probes in shedding light on the analogous enzymatic pathways. Although heme dioxygenase model systems have been recently described in detail,[71−74] indole monooxygenating heme models are still in their infancies, and a clear understanding of the precise mechanistic subtleties and identities of exact active oxidants is acutely lacking.[75,76] Recall that several heme enzyme-mediated indole monooxygenation pathways (and/or their products) hold significant/demonstrated therapeutic utility, highlighting a pressing demand for well-defined indole monooxygenating heme model systems. Perhaps such bioinspired heme model systems also have great prospects for evolving into efficient, selective indole monooxygenation catalysts, with the added benefit of being inexpensive and environmentally benign. Indeed, a majority of current synthetic protocols utilized for the direct conversion of indoles to oxindoles suffer from numerous limitations including narrow substrate scopes and poor selectivity and sustainability.[77−79]

We herein describe the biomimetic oxidation of a variety of indole substrates with variable substituents (Scheme 1), using compound-I (Cmpd-I), compound-II (Cmpd-II), and a protic Lewis acid (i.e., 2,6-lutidinium triflate; [LuH]OTf) activated Cmpd-II species ([(Por)Cmpd-II···(LuH^+)]). To the best of our knowledge, this report marks the first instance where indole monooxygenation capabilities of synthetic high-valent heme-oxo species are being evaluated, revealing key mechanistic insights with relevance to the related enzymatic systems (Figure 1C). Interestingly, our findings demonstrate how Lewis acids can turn on the indole oxidation pathway of Cmpd-II (naked Cmpd-II is inactive toward indole monooxygenation), further confirming the long-predicted importance of secondary sphere noncovalent architectures (e.g., hydrogen bonding) of heme enzyme active sites that fine-tune the chemistries of their important reaction intermediates/active species.[80] In detail, kinetic, thermodynamic, and mechanistic studies are also presented, which reveal the rate-limiting formation of a putative indole epoxide reaction intermediate that rearranges with a 2,3-hydride shift (drawing parallels to cytochrome P450[31] and MarE[36]) to result in the final 2-oxindole product. Hence, this work presents (1) a clear biomimetic mechanistic viewpoint for high-valent heme-mediated indole monooxygenation, highlighting its potential synthetic utility, and (2) a detailed characterization of the reaction mechanism that clearly elucidates critical structure−function relationships. This knowledge will significantly improve the current understanding of heme enzyme mediated indole monooxygenation pathways and will enhance their prospects in future therapeutic target studies. Most importantly, this bioinspired protocol exhibits multifarious benefits that may offer promising leads for its synthetic utility in future: (1) clean and high-yielding pathway for achieving synthetically challenging 2-oxindole targets, (2) efficient/quick and operates under fairly straightforward reaction conditions, and (3) encompasses a broad scope of indole ring substituents within its substrate variability.

RESULTS AND DISCUSSION

Formation and Characterization of Cmpd-I ([(Por)-Cmpd-I]), Cmpd-II ([(Por)Cmpd-II]), and Lewis Acid Activated Cmpd-II ([(Por)Cmpd-II···(LuH^+)]) Complexes. The preparation of [(Por)Cmpd-I] (where Por = tetrakis(2,6-difluorophenyl)porphyrinate (F_8TPP) or 5,10,15,20-(tetramesityl)porphyrinate (TMP)), [(Por)Cmpd-II] (where Por = tetrakis(2,6-difluorophenyl)porphyrinate (F_8TPP)), and [(Por)Cmpd-II···(LuH^+)] species were carried out following previously established methods under paralleled reaction conditions.[81,82] In that, the addition of 2 equiv of *meta*-chloroperbenzoic acid (*m*CPBA) or iodosylbenzene (PhIO) to the naked heme ferric precursor, $[(Por)Fe^{III}]SbF_6$, at −90 °C in degassed dichloromethane initiated the generation of the corresponding [(Por)Cmpd-I] complexes (Scheme S1), which have been unambiguously characterized using UV−vis, ^{2}H NMR, and electron paramagnetic resonance (EPR) spectroscopic methods (Figures S1−S6). For example, $[(F_8TPP)$-Cmpd-I] exhibited characteristic electronic absorption spectral features at 394 (low-intensity Soret band), 592, and 656 nm (relatively intense low-energy band; Figure S1). Low-temperature ^{2}H NMR analyses (at −90 °C) performed using the pyrrole position deuterated F_8TPP-d_8 porphyrinate exhibited a paramagnetically upfield shifted pyrrole-β signal at $\delta_{pyrrole}$ = −78.8 ppm for $[(F_8TPP$-$d_8)$Cmpd-I] (Figure S2),[81,83] and the EPR signatures of $[(F_8TPP)$Cmpd-I] (Figure S3) indicate a quartet ground state (i.e., $S = 3/2$), which are in excellent agreement with previous reports.[83] A similar spectroscopic profile was also obtained for [(TMP)Cmpd-I] (Figures S4−S6).[83,84] $[(F_8TPP)$Cmpd-II] was generated by the addition of 1 equiv of *m*CPBA into a 1:9 THF:toluene solution of $[(F_8TPP)Fe^{II}]$ at −40 °C (Scheme S1) and was monitored by electronic absorption spectroscopy. Therein, clear changes in absorption features were observed from 422 (Soret) and 542 to 415 (Soret) and 544 nm upon the addition of the oxidant (Figure S1). The subsequent addition of 1 equiv of [LuH]OTf to $[(F_8TPP)$Cmpd-II] generated the Lewis acid adduct complex, $[(F_8TPP)$Cmpd-II···$(LuH^+)]$, which was accompanied by a minor change in electronic absorption from 415 (Soret) and 544 to 413 (Soret) and 546 nm (Figure S1). In consistence, a single ^{2}H NMR feature at $\delta_{pyrrole}$ = 3.2 and 4.6 ppm was observed for $[(F_8TPP$-$d_8)$Cmpd-II] and $[(F_8TPP$-$d_8)$Cmpd-II···$(LuH^+)]$, respectively (Figure S7), while both complexes were found to be EPR silent (Figure S8). These characterization details closely resemble those of recent reports.[82,85]

Indole Monooxygenation Reactivities of [(Por)Cmpd-I], $[(F_8TPP)$Cmpd-II], and $[(F_8TPP)$Cmpd-II···$(LuH^+)]$ Complexes. [(Por)Cmpd-I], $[(F_8TPP)$Cmpd-II], and $[(F_8TPP)$-Cmpd-II···$(LuH^+)]$ complexes were probed using a series of differently substituted indole substrates. When 5 equiv of 3-methylindole (**1h**) was added into either $[(F_8TPP)$Cmpd-I] or [(TMP)Cmpd-I] at −90 °C in dichloromethane, the immediate disappearance of the [(Por)Cmpd-I] electronic absorption features was evidenced, with concomitant formation of the corresponding 2-oxindole product (*vide infra*) and the parent ferric heme complex. For example, when [(TMP)Cmpd-I] was reacted with 5 equiv of 3-methylindole, the UV−vis features shifted from 398 and 660 to 396, 498, and 520 nm within 1 min (Figure 2A; see Figure S9 for $[(F_8TPP)$Cmpd-I]). This extremely rapid reactivity of [(Por)-Cmpd-I] complexes thwarted any detailed kinetic analysis; however, we successfully measured the reaction rate for one of the slowest reactions of [(Por)Cmpd-I] (i.e., [(TMP)Cmpd-I] plus 5 equiv of 5-bromoindole (**1d**)) by monitoring the absorbance change at 660 nm immediately following the addition of substrate, which was found to be $24 \pm 0.5 \times 10^{-3}$ s^{-1} (Figure 2A inset). The corresponding control reactions did not produce any 2-oxindole products; that is, when either the (1) heme complex or (2) *m*CPBA oxidant is absent in the reaction mixture, indole monooxygenation reactions did not proceed to produce the expected 2-oxindole product (Figures S10−S12); indeed, bulk scale reactions further corroborate this

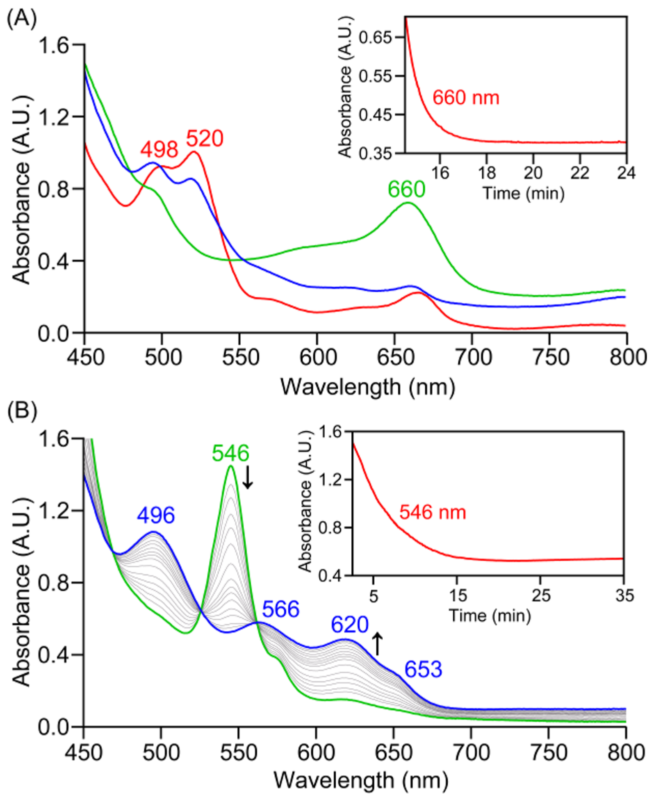

Figure 2. UV−vis spectra for (A) 0.1 mM solution of $[(TMP)Fe^{III}]$-SbF_6 (red), [(TMP)Cmpd-I] (green), and after the addition of 5 equiv of **1h** (blue; i.e., the final heme product) at −90 °C in dichloromethane; inset shows the kinetic time trace collected at 660 nm for [(TMP)Cmpd-I] and 5 equiv of **1d**. (B) Reactivity between a 0.1 mM solution of $[(F_8TPP)$Cmpd-II···$(LuH^+)]$ (green) and 100 equiv of **1a** at −40 °C in 1:9 THF:toluene (final heme product is shown in blue); inset shows the kinetic time trace at 546 nm, and arrows indicate the direction of peak transition.

observation. Importantly, these observations confirm that the *m*CPBA oxidant does not directly react with indole substrates under the conditions employed herein.

On the contrary, no reaction was observed between $[(F_8TPP)$Cmpd-II] and any indole substrate, even after prolonged monitoring at −40 °C (Figure S13); in support, no oxindole product was observed in scaled up/bulk reactions. This resembles previous reports emphasizing the weaker oxidizing capability of Cmpd-II when compared to Cmpd-I.[37] Strikingly, the Lewis acid activated Cmpd-II species, $[(F_8TPP)$Cmpd-II···$(LuH^+)]$, immediately initiates reactivity with indole substrates giving the desired 2-oxindole products (*vide infra*),[86] although at much slower rates in comparison to Cmpd-I. The slower reaction rates of $[(F_8TPP)$Cmpd-II···$(LuH^+)]$ allowed the detailed kinetic and thermodynamic elucidation of its indole monooxygenation reactivity. In that, the addition of 100 equiv of indole (**1a**) into a solution of $[(F_8TPP)$Cmpd-II···$(LuH^+)]$ in 1:9 THF:toluene at −40 °C resulted in the gradual disappearance of its electronic absorption features exhibiting a first-order decay profile (Figure 2B and Figure S9). The pseudo first-order rate constants determined by fitting the kinetic time traces for the decay of $[(F_8TPP)$Cmpd-II···$(LuH^+)]$ increased linearly with indole substrate concentrations, affording a second-order rate constant (k_2) of 0.47 ± 0.05 M^{-1} s^{-1} at −40 °C (Figure 3A). Identical spectral changes were observed for the reactions

https://doi.org/10.1021/jacs.1c11068
J. Am. Chem. Soc. XXXX, XXX, XXX−XXX

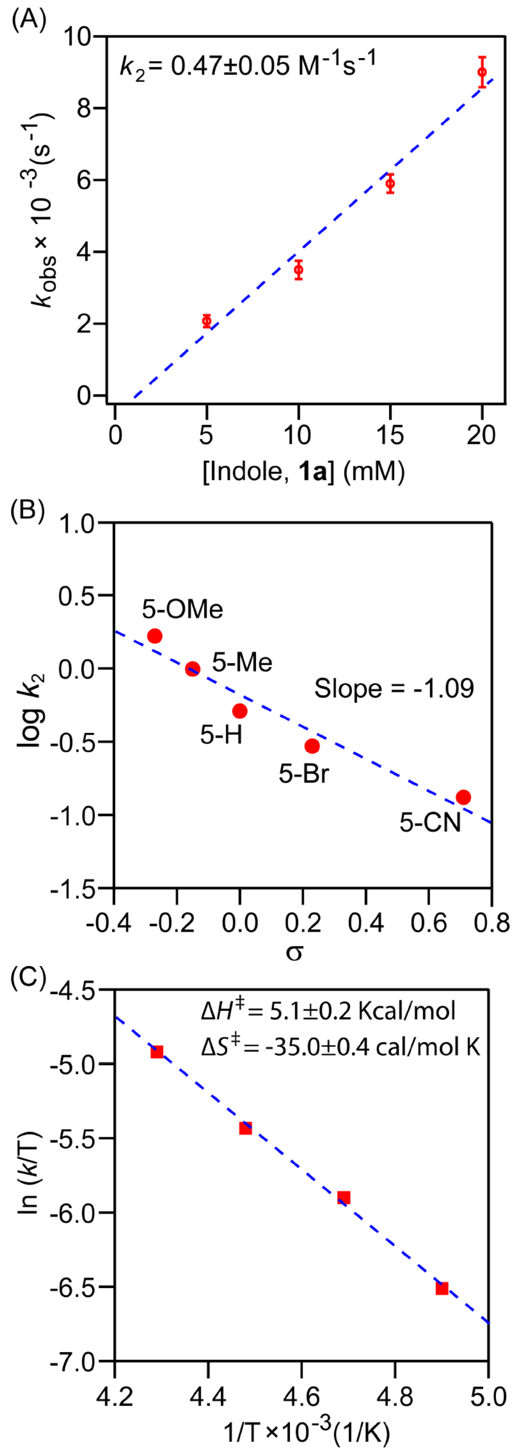

Figure 3. (A) Plot of pseudo-first-order rate constants (k_{obs}) versus [**1a**] for a 0.1 mM solution of [(F_8TPP)Cmpd-II···(LuH^+)] at −40 °C. (B) Plot of log k_2 versus σ for the reactions between [(F_8TPP)Cmpd-II···(LuH^+)] and 5-substituted-indole substrates at −40 °C. (C) Eyring plot showing ln(k/T) versus $1/T$ for the reaction between 0.1 mM [(F_8TPP)Cmpd-II···(LuH^+)] and 5-methoxyindole (**1b**) carried out at −40, −50, −60, and −70 °C. Solvent: 1:9 THF:toluene.

between [(F_8TPP)Cmpd-II···(LuH^+)] and other indole substrates (**1b**−**1n**) shown in Scheme 1. Moreover, similar to the Cmpd-I situation, control experiments did not result in any oxindole product formation.

To gain further insight into the mechanism, we carried out a Hammett study involving a series of electronically divergent 5-substituted (5-R) indoles (**1a**−**1e**; Scheme 1). This investigation revealed faster second order rate constants with electron rich substrates compared to electron deficient indoles (Figure S14), clearly indicating the capability of electronic effects exerted by 5-R substituents to significantly influence the rate of monooxygenation, i.e., the initial reactivity between the heme oxidant and the indole substrate is overall rate-limiting, as also supported by the pseudo first-order rate constants (Figure 3A). Moreover, a linear correlation was obtained between log k_2 and Hammett parameters (σ) of the substituents,[87] resulting in a slope (ρ value) of −1.09 (Figure 3B), unambiguously divulging the electrophilic character of [(F_8TPP)Cmpd-II···(LuH^+)] in the rate-limiting step. Similar observations have previously been reported for oxo atom transfer (OAT) reactions of heme and nonheme iron(IV or V)-oxo complexes.[22] Notably, our Hammett correlations are in close agreement with a prior study that involved an OsO_4 indole monoxygenating catalyst along with aryl-*N*-haloamine oxidants (ρ = −1.0).[88] While these similarities should be viewed within the caveat of the stark differences in identities of metal complexes, oxidants, as well as the reaction conditions, in both systems, the indole substrate behaves as a nucleophile. We then set out to determine the activation parameters for indole monooxygenation by carrying out variable temperature (Eyring) analysis of kinetic data for reactivities between 5-methoxyindole (**1b**) and [(F_8TPP)Cmpd-II···(LuH^+)] (Figure S14). An Eyring plot is shown in Figure 3C, which afforded an enthalpy ($\Delta H^{\ddagger}$) and entropy ($\Delta S^{\ddagger}$) of activation of 5.1 ± 0.2 kcal mol^{-1} and −35.0 ± 0.4 cal mol^{-1} K^{-1}, respectively. These parameters result in an activation free energy change ($\Delta G^{\ddagger}$) of 13.2 ± 0.2 kcal mol^{-1} at −40 °C. The relatively large, negative activation entropy is consistent with a bimolecular reaction and implicates a highly ordered transition state. Such a transition state would be in line with the observed depletion in the reaction yields upon increased steric encumbrance about the reaction center (*vide infra*). Interestingly, our activation parameter values are in accordance with previously reported values for indole monooxygenation in other systems[89,90] and emphasize the cruciality of noncovalent interactions within metalloprotein active sites that aid in facilitating smooth biological transformations, which, in their absence, could potentially be energetically unfavorable. For example, Arg-38 and His-42 at the distal side of HRP active site have been proposed to stabilize its high-valent intermediates, and in the HRP Cmpd-I crystal structure (as also evidenced among other similar structures[2]), a hydrogen bonding interaction is clearly evident between the Fe(IV)=O unit and Arg-38.[91] Moreover, His-55 at the DHP distal site has been found to be essential for its peroxidase functionality.[28]

Mechanistic Studies and Product Characterization. A clear comprehension of the precise mechanistic landscape of indole monooxygenation by high-valent heme-oxo intermediates is extremely important due to its direct relevance in multiple heme enzymes in biology and the emerging significance of those systems in human disease and therapy. First, we elucidated the source of the oxygen atom in monooxygenated products by using isotopically labeled heme oxidants. In that, ^{18}O-labeled [(F_8TPP)Cmpd-I] was reacted with 3-methylindole at −40 °C, and the ^{18}O isotope distribution was mapped via product analysis by LC-MS. A high yielding ^{18}O label incorporation (~80%)[92] into the corresponding product, 3-methyl-2-oxindole was observed, upon which, its mass shifted from 148.07 to 150.08 *m*/*z* (Figure S15). This unambiguously confirms that the sole source of oxygen for the final product is indeed the high-valent heme-oxo complex. Furthermore, in support, when indole substrates were oxidized via nonlabeled heme-oxo oxidants but under an $^{18}O_2$ atmosphere, the product did not contain any ^{18}O-label, corroborating that atmospheric O_2 gas is not involved in the mechanism. Accordingly, an indole epoxide intermediate is most likely occurring (i.e., via an initial OAT from high-valent heme-oxo species as also supported by Hammett studies), and a subsequent hydride migration from C_2- to C_3-position on the indole ring could presumably result in the formation of 2-oxindole products (Scheme 2). Similar

Scheme 2. Proposed Mechanistic Pathway for the Monooxygenation of Indole Substrates by Cmpd-I and Activated Cmpd-II Oxidants

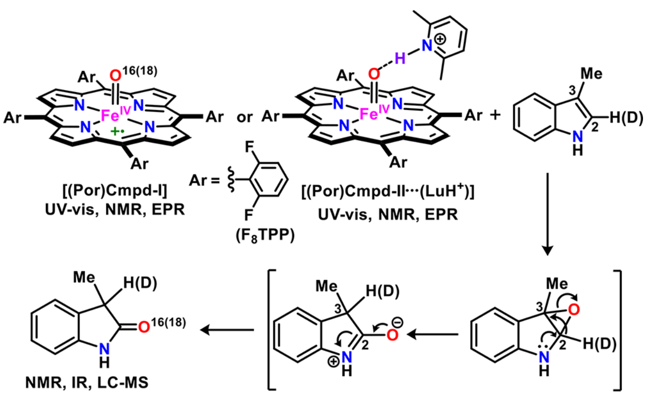

mechanistic proposals have also been described for MarE[36] and Cyt P450[31] enzymes and are in-line with the known decay pathways of indole epoxides.[93] We probed the possibility of such a 2,3-hydride migration utilizing the 2-position deuterated 3-methyindole substrate. Intriguingly, the final product unequivocally contained the deuterium label at the C_3 position (^1H and ^2H NMR; Figures S17 and S18), irrespective of the identity of the oxidant; mass spectrometric analysis confirms deuterium retention (Figure S19). These characterization details clearly illustrate that the hydrogen at C_3 position in the final oxindole product originates from the C_2 position of the starting material, thereby confirming a 2,3-hydride shift of an indole epoxide reaction intermediate that initially forms during the reaction. In summation, the overall reaction mechanism commences with a rate-limiting epoxidation step occurring between the high-valent heme oxidant and the indole substrate, which is followed by a subsequent 2,3-hydride shift in the indole epoxide intermediate to exclusively result in 2-oxindole products (Scheme 2).

To further rationalize and showcase the utility of these synthetic high-valent heme oxidants in monooxygenating variably substituted indole substrates, we have carried out scaled-up reactions using the [(F_8TPP)Cmpd-I] oxidant along with a medley of indole substrates (**1a**−**1n**; Scheme 1). All substrates exclusively resulted in the desired 2-oxindole product with a maximum isolated yield of 88% for 3-methylindole (**1h**);[94] note that this is the same substrate monooxygenated by respiratory Cyt P450 enzymes in humans and is thought to play a role in early stages of lung cancer (*vide supra*).[42,43] The monooxygenated indole products in all cases were rigorously characterized by ^1H and ^{13}C NMR, FT-IR, LC-MS, and ESI-MS methods (Figures S20−S47).[95] Therefore, this bioinspired methodology operates with remarkable selectively and is relatively straightforward and rapid/instantaneous and does not require any harsh experimental conditions. It is applicable to an appreciable range of *N*-, 3-, and 5-substituted indole substrates where the highest yields are observed when the indole 2,3-double bond is most electron rich (**1h**). Electronic effects exerted by the indole 5-position substituents (**1a**−**1e**) also clearly dictate the yields and rates (see above for Hammett analysis), and excessive steric bulk at the 3-position diminishes the final yields presumably due to unfavorable steric encumbrance about the reaction center. This is also supported by the largely negative entropy of activation that substantiates a highly ordered transition state for the rate-limiting step, wherein the heme oxidant and indole substrate would meet in close proximity to mediate epoxidation. The stoichiometric final heme product following monooxygenation by [(Por)Cmpd-I] has been fully characterized to be the "naked" ferric precursor complex, $[(Por)Fe^{III}]^+$, by UV−vis, NMR, and EPR spectroscopies (Figure 2A and Figures S2, S3, S6, and S9; yield: 90%).[81] Interestingly, when [(F_8TPP)Cmpd-II···(LuH^+)] is the oxidant, the final heme product was found to be the corresponding heme ferric aqua complex, $[(F_8TPP)Fe^{III}(OH_2)]^+$ (Figure 2B (blue trace) and Figures S7−S9[85]) rather than the expected Fe(II) complex resulting from the epoxidation reactivity with indoles. As seen in other situations,[96] this is most likely due to the disproportionation of [(F_8TPP)Cmpd-II···(LuH^+)] with $[(F_8TPP)Fe^{II}]$ that results from monooxygenation to finally yield the $[(F_8TPP)Fe^{III}(OH_2)]^+$ product. In support, we (1) only observe substoichiometric yields of 2-oxindole products (∼35%) when [(F_8TPP)Cmpd-II···(LuH^+)] is the oxidant and (2) have carried out control experiments where [(F_8TPP)Cmpd-II···(LuH^+)] readily undergo disproportionation with $[(F_8TPP)Fe^{II}]$ stoichiometrically producing the observed heme ferric aqua product, $[(F_8TPP)Fe^{III}(OH_2)]^+$. Accordingly, the yield of the final $[(F_8TPP)Fe^{III}(OH_2)]^+$ species resulting from indole monooxygenation was found to be 96% (Figure S9).

■ CONCLUSIONS

The direct monooxygenation of indoles to generate oxindoles has accumulated considerable interest in the recent years due its implications in several important areas, such as (1) the significance of such conversions within biological systems for the clear comprehension of pathogenic pathways, thereby making them focal points for rational drug design and (2) the widespread pharmacological applications of oxindole motifs against a broad array of human diseases including cancer. Multiple heme enzymes can mediate the conversion of indoles to oxindoles, albeit only a handful of those exhibit excellent selectivities. A majority of these heme enzyme mechanisms have been proposed to proceed via a Cmpd-I active oxidant; however, a generalized, precise mechanistic understanding is severely lacking, impeding the design of better/targeted therapeutic agents (e.g., inhibitors). Such knowledge would also benefit the development of efficient, sustainable routes for the generation of oxindole pharmacophores, which have already been incorporated into marketed drugs and current drug candidates (*vide supra*). A carefully designed biomimetic synthetic model system could effectively address this demand, and in fact, the indole monooxygenation chemistry of well-

https://doi.org/10.1021/jacs.1c11068
J. Am. Chem. Soc. XXXX, XXX, XXX−XXX

defined high-valent synthetic heme oxidants (such as Cmpd-I and Cmpd-II) has not been described until now. To this end, this study presents two examples of Cmpd-I intermediates with varying electronic properties that efficiently and rapidly monooxygenate indole substrates with no perceivable limitations in substate scope, to exclusively produce the corresponding 2-oxindole product. Cmpd-II intermediate studied herein is unreactive toward indoles by itself; however, upon activation via a secondary sphere Lewis acid interaction, the resulting Cmpd-II···Lewis acid adduct readily monooxygenates indoles to result in the same 2-oxindole product as Cmpd-I, although at much slower rates.

Detailed thermodynamic, kinetic (rate, Hammett, and Eyring analyses), and mechanistic (isotope-labeled (i.e., ^{18}O-labeled oxidants and ^{2}H-labeled substrate) analyses and comparison of differently substituted oxindole yields) studies are also presented for these heme oxidants, all of which point to a rate-limiting epoxidation process (kinetic and Hammett analyses)[97] that initially takes place between the heme oxidant and the indole substrate resulting in the formation of an indole epoxide reaction intermediate. This intermediate rearranges via a 2,3-hydride shift, which results in epoxide ring opening and formation of the final 2-oxindole product (Scheme 2). The yields and rates of these reactions vary with respect to indole ring substituents, underscoring crucial electronic and steric effects that are in excellent agreement with the aforementioned proposed reaction pathway. These mechanistic findings and structure−function relationships shine light on key unknowns pertaining to therapeutically important indole monooxygenating pathways of heme enzymes. Additionally, these model systems are promising candidates for pursuing superior indole monooxygenating synthetic systems that can produce outstanding yields of oxindoles along with a broad substrate scope and remarkable economical and environmental sustainability. Nevertheless, precise optimization of these systems for high-throughput synthetic applications is far from complete, and some key unknowns to be tackled include the evaluation of the robustness of these systems under variable reaction conditions (such as solvent properties (e.g., polarity, pH, protic/aprotic) and reaction temperatures, etc.), as well as revealing how various oxidants, and heme-based properties (electronic effects exerted by the supporting porphyrinate, heme axial ligation, and secondary sphere noncovalent interactions) would modulate the mechanism at play, thereby modifying the overall versatility and efficiency of indole monooxygenation.

■ EXPERIMENTAL SECTION

Materials and Methods. All commercially available chemicals were purchased at the highest available purity and used as received unless otherwise stated. Air-sensitive compounds were handled either under an argon atmosphere using standard Schlenk techniques or in an MBraun Unilab Pro SP (<0.1 ppm of O_2, <0.1 ppm of H_2O) nitrogen-filled glovebox. All organic solvents were purchased at HPLC-grade or better and degassed (bubbling argon gas for 40 min at room temperature) and dried (passing through a 60 cm alumina column) using an Inert Pure Solv MD 5 (2018) solvent purification system. These solvents were then stored in amber glass bottles inside the glovebox over 4 Å molecular sieves at least for 72 h prior to use. The oxidant, 3-chloroperbenzoic acid (*m*CPBA), was purified according to published procedures.[98] Benchtop UV−vis experiments were carried out using an Agilent Cary 60 spectrophotometer equipped with a liquid nitrogen chilled Unisoku CoolSpek UV USP-203-B cryostat. A 10 mm path length quartz cell cuvette modified with an extended glass neck with a female 14/19 joint and stopcock was used to perform all UV−vis experiments. Low-temperature ^{1}H and ^{2}H NMR spectroscopic studies were carried out on Bruker AV 400 and Bruker AV 360 MHz NMR spectrometers. All spectra were recorded in 5 mm (outer diameter) NMR tubes. The chemical shifts were reported as δ (ppm) values calibrated to natural abundance deuterium or proton solvent peaks. Infrared (IR) vibrational spectra were collected on a Bruker FT-IR spectrometer (Vertex 70) at room temperature. For LC-MS analysis, a SCIEX 5600 Triple-Tof (time-of-flight) mass spectrometer (SCIEX, Toronto, Canada) was used to analyze the mass profiles of the organic products. The IonSpray voltages for positive modes were ±5000 V, and the declustering potential was 80 V. Ionspray GS1/GS2 and curtain gases were set at 40 and 25 psi, respectively. The interface heater temperature was maintained at 400 °C. ESI-MS data were collected on a Waters Xevo G2-XS Qtof (quadrupole time-of-flight) instrument, and the conditions are capillary voltage at 0.8 kV in positive mode, sampling cone at 40 V, source offset at 80, source temperature at 100 °C, desolvation at 350 °C, cone gas at 30 L/h, desolvation gas at 400 L/h, lock spray capillary voltage at 0.1 kV, and lock mass at 556.2771 in positive mode (leucine enkephalin). The expected cations or $[M + H]^+$ or $[M + Na]^+$ ions were observed in positive ion mode with <5 ppm mass accuracy. Electron paramagnetic resonance (EPR) spectra were collected in 4 mm (outer diameter) quartz tubes using an X-band Bruker EMX-plus spectrometer coupled to a Bruker ER 041 XG microwave bridge and a continuous-flow liquid helium cryostat (ESR900) controlled by an Oxford Instruments TC503 temperature controller (experimental conditions: microwave frequency = 9.41 GHz; microwave power = 0.2 mW; modulation frequency = 100 kHz; modulation amplitude = 10 G; temperature = 7 K). The syntheses of $H_2(F_8TPP)$,[99] $H_2(F_8TPP\text{-}d_8)$,[99] $H_2(TMP)$,[100] 1,3-dimethylindole (**1g**),[101] 2-deuterated 3-methyindole,[102] tosylated tryptamine (**1l**),[103] and [LuH]OTf[104] were carried out according to previously published methods. Metalation of the porphyrinates to generate $[(F_8TPP)Fe^{III}Cl]$, $[(F_8TPP\text{-}d_8)Fe^{III}Cl]$ and $[(TMP)Fe^{III}Cl]$ and their corresponding "naked" complexes, $[(F_8TPP)Fe^{III}]SbF_6$, $[(F_8TPP\text{-}d_8)Fe^{III}]SbF_6$, and $[(TMP)Fe^{III}]SbF_6$, were synthesized as previously reported.[99,105] The reduction of $[(F_8TPP)Fe^{III}Cl]$ to $[(F_8TPP)Fe^{II}]$ was carried out by following previously reported procedures.[99]

Formation of [(Por)Cmpd-I], [(F_8TPP)Cmpd-II], and the Lewis Acid Adduct [(F_8TPP)Cmpd-II···(LuH^+)] Complexes (Por = Porphyrinate Supporting Ligand). The generation of the [(Por)Cmpd-I] (where Por = F_8TPP and TMP) complexes was carried out following a literature-adapted procedure.[81] In a typical experiment, a 0.1 mM dichloromethane solution (3.0 mL) of $[(Por)Fe^{III}]SbF_6$ was added into a 10 mm path length Schlenk cuvette inside the glovebox and was sealed using a rubber septum. Upon cooling inside the UV−vis cryostat stabilized at −90 °C for 10 min, the addition of 2 equiv of *m*CPBA (25 μL in dichloromethane) resulted the formation of corresponding [(Por)Cmpd-I] complexes over ∼15 min (Figures S1 and S4).

Similarly, [(F_8TPP)Cmpd-II] and its Lewis acid (i.e., 2,6-lutidinium triflate; [LuH]OTf) adduct, [(F_8TPP)Cmpd-II···(LuH^+)], were synthesized as previously described.[82] A 0.1 mM 1:9 THF:toluene solution (3.0 mL) of $[(F_8TPP)Fe^{II}]$ was taken in a 10 mm path length Schlenk cuvette and sealed with a rubber septum inside the glovebox. This cuvette was then cooled in the UV−vis cryostat to −40 °C for 10 min. Upon thermal equilibration, 1 equiv of *m*CPBA (25 μL in toluene) was added to generate [(F_8TPP)Cmpd-II]. Subsequent addition of 1 equiv of [LuH]OTf (25 μL in 1:9 THF:toluene) to [(F_8TPP)Cmpd-II] resulted in the formation of the Lewis acid adduct complex, [(F_8TPP)Cmpd-II···(LuH^+)] (Figure S1).

Kinetic Studies of [(TMP)Cmpd-I] with Indole Substrate (1d). For kinetic experiments, a 0.1 mM dichloromethane solution (3 mL) of [(TMP)Cmpd-I] intermediate was generated at −90 °C in a 10 mm path length Schlenk cuvette as described above. Then, 5 equiv of the indole substrate (25 μL in dichloromethane) was added into the cuvette using a Hamilton gastight syringe, and the reaction mixture was quickly mixed with argon bubbling. The reaction was monitored by the progression of spectral changes centered at 660 nm using the single wavelength scan mode (Figure 2A). The pseudo-first-order rate constant, k_{obs} was calculated from the plot of $\ln[(A - A_f)/(A_i - A_f)]$ vs time(s), where A_i and A_f are initial and final absorbances, respectively.

Spectroscopic Reactivity and Kinetic Studies of [(F_8TPP)-Cmpd-II···(LuH^+)] with Indole Substrates. In a typical kinetic experiment, a 0.1 mM 1:9 THF:toluene solution (3 mL) of [(F_8TPP)Cmpd-II···(LuH^+)] was prepared in a 10 mm path length Schlenk cuvette as described above. Subsequently, the indole substrate (25 μL in 1:9 THF:toluene) was added into the cuvette using a gastight syringe, and the reaction mixture was quickly mixed with argon bubbling. The reaction was monitored by the progression of spectral changes centered at 546 nm until plateaued. Kinetic studies were carried out under pseudo-first-order conditions by the addition of 50−200 equiv of indole substrates (**1a**−**1e**) into a 0.1 mM 1:9 THF:toluene solution (3 mL) of [(F_8TPP)Cmpd-II···(LuH^+)] at −40 °C. For Eyring analysis, kinetic experiments between [(F_8TPP)Cmpd-II···(LuH^+)] and 5-methoxyindole (**1b**) were carried out at variable temperatures (i.e., −40, −50, −60, and −70 °C) as described above. The pseudo-first-order rate constants, k_{obs} were calculated from plots of $\ln[(A - A_f)/(A_i - A_f)]$ vs time(s), where A_i and A_f are initial and final absorbances, respectively. The second-order rate constants (k_2) were obtained from the slope of the best-fit line from a plot of k_{obs} values vs substrate concentration (Figure S14).

Low-Temperature ^{2}H NMR Spectroscopic Studies. For a typical ^{2}H NMR experiment, [(F_8TPP-d_8)Fe^{III}]SbF_6 (16 mg, 0.015 mmol) or [(F_8TPP-d_8)Fe^{II}] (12 mg, 0.014 mmol) was dissolved in 0.5 mL of degassed DCM (or 1:9 THF:toluene) in a 5 mm (outer diameter) NMR tube inside the glovebox and was sealed with a rubber septum. This tube was then stabilized at −90 °C or (−40 °C) using a liquid nitrogen/acetone cold bath, followed by the addition of 2 or 1 equiv of *m*CPBA (25 μL in DCM or toluene) to generate the corresponding [(F_8TPP-d_8)Cmpd-I] or [(F_8TPP-d_8)Cmpd-II] complexes. Final reactivity products were generated by subsequent addition of substrates (in DCM or toluene) into [(F_8TPP-d_8)Cmpd-I] or [(F_8TPP-d_8)Cmpd-II···(LuH^+)] complexes. Immediately following the completion of the reaction, the tube was transferred into the cryostat of the NMR spectrometer held at −90 °C (or −40 °C) (Figures S2 and S7).

EPR Sample Preparation. EPR samples were prepared similarly to UV−vis samples as mentioned earlier; EPR sample concentration was 2 mM in dichloromethane (for [(Por)Cmpd-I]) or in 1:9 THF:toluene (for [(F_8TPP)Cmpd-II] and [(F_8TPP)Cmpd-II···(LuH^+)]) prepared at −90 °C (or −40 °C; i.e., using an acetone/liquid N_2 cold bath) in a 4 mm outer diameter quartz EPR tube. These tubes were immediately frozen in liquid N_2 following the completion of the desired reaction. All measurements were carried out at 7 K (Figures S3, S6, and S8).

Scaled-Up Monooxygenation Reactions and Characterization of Organic Products. Bulk monooxygenation reactions for all indole substrates were carried out using [(F_8TPP)Cmpd-I] following a generalized procedure as follows: a 25 mL Schlenk flask containing [(F_8TPP)Fe^{III}]SbF_6 (200 mg, 0.19 mmol) in dichloromethane (10 mL) under inert gas was cooled to −90 °C in an acetone/liquid N_2 cold bath. Upon temperature equilibration, 2 equiv of *m*CPBA (in 0.2 mL of dicholoromethane) was added in to form [(F_8TPP)Cmpd-I]. Then, 3-methylindole, **1h** (25 mg, 0.19 mmol; in 0.2 mL of dichloromethane), was added in, and the color of the reaction mixture immediately changed from emerald green to brown. The reaction mixture was stirred for another 15 min at −90 °C before it was dried in a vacuum, and the final 2-oxindole (organic) product (**2h**) was purified by silica gel column chromatography using EtOAc/hexane (1:1) as the eluent. 2,3-deuterium migration experiment was carried out following the above procedure using [(F_8TPP)Cmpd-I] and 2-deuterated 3-methyindole as the substrate. The ^{18}O-labeled experiment was also performed in a similar manner by adding **1h** to a reaction mixture (at −40 °C in dichloromethane) containing [(F_8TPP)Fe^{III}]SbF_6 and $PhI^{18}O$, which was prepared by treating PhIO (2 equiv dissolved in 100 μL acetonitrile) with $H_2{}^{18}O$ (100 μL, 98% ^{18}O enriched).[106]

2a. Yield: 21 mg (80%). ^{1}H NMR ($CDCl_3$, 298 K): δ = 9.33 (br, 1 H), 7.24 (t, 2H), 7.04 (t, 1H), 6.93 (d, 1H), 3.57 (s, 2H). ^{13}C NMR (125 MHz, $CDCl_3$, 298 K): δ (ppm) = 178.3, 142.6, 127.9, 125.2, 124.5, 122.3, 109.9, 36.3. FT-IR (ATR, cm^{-1}): 1688, 1615, 1468, 1384, 1232, 1211, 746. ESI-MS: $[M + H]^+$ m/z = 134.06 (calc. 134.06).

2b. Yield: 26 mg (85%). ^{1}H NMR ($CDCl_3$, 298 K): δ (ppm) = 8.92 (br, 1H), 6.87 (m, 1H), 6.82 (d, 1H), 6.77 (d, 1H), 3.80 (s, 3 H), 3.55 (s, 2H). ^{13}C NMR (125 MHz, DMSO-d_6, 298 K): δ (ppm) = 176.6, 155.0, 137.5, 127.5, 112.6, 111.9, 109.7, 55.8, 36.6. FT-IR (ATR, cm^{-1}): 1686, 1605, 1487, 1464, 1387, 1316, 1278, 1224, 1198, 1185, 1136, 851, 790, 712, 670. ESI-MS: $[M + H]^+$ m/z = 164.07 (calc. 164.07).

2c. Yield: 23 mg (82%). ^{1}H NMR ($CDCl_3$, 298 K): δ (ppm) = 8.99 (br, 1H), 7.06−7.03 (m, 2H), 6.81 (dd, 1H), 3.53 (s, 2H), 2.34 (s, 3H). ^{13}C NMR (125 MHz, DMSO-d_6, 298 K): δ (ppm) = 176.7, 141.6, 130.3, 128.0, 126.3, 125.5, 109.2, 36.6, 21.1. FT-IR (ATR, cm^{-1}): 1685, 1621, 1486, 1390, 1260, 1191, 1128, 851, 795, 669. ESI-MS: $[M + H]^+$ m/z = 148.07 (calc. 148.07).

2d. Yield: 31 mg (78%). ^{1}H NMR ($CDCl_3$, 298 K): δ (ppm) = 8.17 (br, 1H), 7.19−7.16 (m, 2H), 6.63 (d, 1H), 3.35 (s, 2H). ^{13}C NMR (125 MHz, $CDCl_3$, 298 K): δ (ppm) = 176.3, 143.4, 130.5, 128.9, 127.6, 113.2, 111.3, 36.2. FT-IR (ATR, cm^{-1}): 1727, 1694, 1471, 1409, 1375, 1308, 1238, 1166, 812, 746. ESI-MS: $[M + H]^+$ m/z = 211.97 (calc. 211.97).

2e. Yield: 22 mg (75%). ^{1}H NMR (DMSO-d_6, 298 K): δ (ppm) = 10.85 (br, 1H), 7.63 (br, 2H), 6.95 (br, 1H), 3.56 (s, 2H). ^{13}C NMR (125 MHz, DMSO-d_6, 298 K): δ (ppm) = 176.7, 148.6, 133.4, 128.2, 127.6, 120.0, 110.2, 103.5, 35.8. FT-IR (ATR, cm^{-1}): 2221, 1711, 1624, 1485, 1318, 1248, 1109, 822, 670. ESI-MS: $[M + H]^+$ m/z = 159.05 (calc. 159.05).

2f. Yield: 22 mg (81%). ^{1}H NMR ($CDCl_3$, 298 K): δ (ppm) = 7.20−7.16 (m, 2H), 6.97 (t, 1H), 6.74 (d, 1H), 3.45 (s, 2H), 3.14 (s, 3H). ^{13}C NMR (125 MHz, $CDCl_3$, 298 K): δ (ppm) = 175.0, 145.2, 127.9, 124.5, 124.3, 122.3, 108.0, 35.7, 26.1. FT-IR (ATR, cm^{-1}): 1698, 1606, 1463, 1425, 1370, 1311, 1124, 1091, 743. ESI-MS: $[M + H]^+$ m/z = 148.07 (calc. 148.07).

2g. Yield: 25 mg (80%). ^{1}H NMR ($CDCl_3$, 298 K): δ (ppm) = 7.30−7.25 (m, 2H), 7.08 (t, 1H), 6.85 (d, 1H), 3.45 (q, 1H), 3.23 (s, 3H), 1.48 (d, 3H). ^{13}C NMR (125 MHz, $CDCl_3$, 298 K): δ (ppm) = 178.6, 143.9, 130.6, 127.8, 123.4, 122.3, 107.9, 40.5, 26.1, 15.3. FT-IR (ATR, cm^{-1}): 1700, 1608, 1467, 1373, 1345, 1219, 1124, 747. ESI-MS: $[M + H]^+$ m/z = 162.09 (calc. 162.09).

2h. Yield: 25 mg (88%). ^{1}H NMR ($CDCl_3$, 298 K): δ (ppm) = 8.95 (br, 1 H), 7.23 (t, 2H), 7.05 (m, 1H), 6.94 (d, 1H), 3.48 (q, 1H), 1.52 (d, 3H). ^{13}C NMR (125 MHz, $CDCl_3$, 298 K): δ (ppm) = 181.9, 141.4, 131.3, 127.9, 123.7, 122.3, 109.9, 41.1, 15.2. FT-IR (ATR, cm^{-1}): 1697, 1618, 1486, 1334, 1224, 1212, 747. ESI-MS: $[M + H]^+$ m/z = 148.07 (calc. 148.07).

2i. Yield: 28 mg (85%). ^{1}H NMR ($CDCl_3$, 298 K): δ (ppm) = 8.34 (br, 1H), 7.51 (d, 1H), 7.36−7.33 (m, 1H), 7.14 (m, 1H), 6.96 (d, 1H), 3.73 (dd, 1H), 3.12 (dd, 1H), 2.78 (dd, 1H). ^{13}C NMR (125 MHz, $CDCl_3$, 298 K): δ (ppm) = 176.6, 141.6, 129.6, 126.3, 124.6, 123.3, 117.4, 110.5, 42.0, 19.0. FT-IR (ATR, cm^{-1}): 1702, 1618, 1469, 1339, 1236, 1217, 746. ESI-MS: $[M + Na]^+$ m/z = 195.05 (calc. 195.05).

2j. Yield: 33 mg (80%). ^{1}H NMR ($CDCl_3$, 298 K): δ (ppm) = 8.73 (br, 1H), 7.28−7.24 (m, 2H), 7.03 (t, 1H), 6.93 (t, 1H), 4.17 (m, 2H), 3.83 (dd, 1H), 3.12−3.08 (m, 1H), 2.88−2.84 (m, 1H) 1.23 (m, 3H). ^{13}C NMR (125 MHz, $CDCl_3$, 298 K): δ (ppm) = 179.4, 171.0, 141.6, 128.7, 128.3, 124.0, 122.4, 109.9, 61.0, 42.4, 34.8, 14.1. FT-IR (ATR, cm^{-1}): 1725, 1698, 1618, 1469, 1336, 1236, 1164, 747. ESI-MS: $[M + Na]^+$ m/z = 242.07 (calc. 242.07).

2k. Yield: 26 mg (78%). ^{1}H NMR ($CDCl_3$, 298 K): δ (ppm) = 8.64 (br, 1H), 7.29−7.24 (m, 2H), 7.07 (t, 1H), 6.92 (d, 1H), 3.92 (t, 2H), 3.65 (dd, 1H), 2.26 (m, 1H), 2.12 (m, 1H). ^{13}C NMR (125 MHz, $CDCl_3$, 298 K): δ (ppm) = 181.3, 141.2, 129.4, 128.1, 124.0, 122.6, 109.9, 60.7, 44.7, 33.1. FT-IR (ATR, cm^{-1}): 1680, 1614, 1469, 1345, 1209, 1034, 756. ESI-MS: $[M + Na]^+$ m/z = 200.06 (calc. 200.06).

https://doi.org/10.1021/jacs.1c11068
J. Am. Chem. Soc. XXXX, XXX, XXX−XXX

2l. Yield: 47 mg (75%). ^{1}H NMR ($CDCl_3$, 298 K): δ (ppm) = 7.96 (br, 1H), 7.75 (d, 2H), 7.30−7.28 (m, 3H), 7.18 (t, 1H), 7.06 (t, 1H), 6.88 (d, 1H), 5.58 (m, 1H), 3.52 (m, 1H), 3.24−3.16 (m, 2H), 2.43 (s, 3H), 2.22 (m, 1H), 2.01 (m, 1H). ^{13}C NMR (125 MHz, $CDCl_3$, 298 K): δ (ppm) = 180.5, 143.4, 141.2, 137.0, 129.7, 129.7, 128.6, 127.1, 124.1, 122.7, 110.3, 43.8, 40.8, 30.9, 21.5. FT-IR (ATR, cm^{-1}): 1693, 1596, 1468, 1318, 1214, 1154, 1061, 745, 656. ESI-MS: $[M + Na]^+$ m/z = 353.09 (calc. 353.09).

2m. Yield: 33 mg (72%). ^{1}H NMR (DMSO-d_6, 298 K): δ (ppm) = 10.22 (br, 1H; NH), 7.93 (br, 1H; N−H), 6.97 (br, 1H; −Ar−H), 6.74 (m, 2H; Ar−H), 3.70 (s, 3H; $-OCH_3$), 3.21 (m, 1H; $-CH_2$) 3.07 (m, 1H; $-CH_2$), 1.97 (m, 1H; $-CH_2$), 1.78 (m, 4H; $-CH_3$ and − CH). ^{13}C NMR (125 MHz, DMSO-d_6, 298 K): δ (ppm) = 178.9, 169.6, 154.8, 136.6, 131.3, 112.7, 111.8, 109.9, 55.8, 43.9, 36.1, 30.7, 23.1. FT-IR (ATR, cm^{-1}): 1690, 1639, 1479, 1366, 1212, 1031, 788, 602. ESI-MS: $[M + Na]^+$ m/z = 271.10 (calc. 271.10).

2n. Yield: 37 mg (70%). ^{1}H NMR ($CDCl_3$, 298 K): δ (ppm) = 8.87 (br, 1H), 7.42 (t, 1H), 7.23 (t, 1.5H), 7.07 (m, 1H), 6.96 (br, 0.5H), 6.90 (m, 1H), 4.94 (m, 0.5H), 4.76 (m, 0.5H), 3.77 (s, 1.5H), 3.70 (s, 1.5H), 3.60−3.53 (m, 1H), 2.51 (m, 0.6H), 2.43−2.30 (m, 2.4H), 2.02 (d, 3H). ^{13}C NMR (125 MHz, DMSO-d_6, 298 K): δ (ppm) = 178.5, 173.0, 169.9, 143.1, 129.4, 128.3, 124.8, 121.7, 109.7, 52.2, 50.4, 42.5, 32.2, 22.7. FT-IR (ATR, cm^{-1}): 1698, 1541, 1470, 1211, 1173, 750, 662. ESI-MS: $[M + Na]^+$ m/z = 299.10 (calc. 299.10).

■ ASSOCIATED CONTENT

Supporting Information

The Supporting Information is available free of charge at https://pubs.acs.org/doi/10.1021/jacs.1c11068.

Scheme showing the generation of [(Por)Cmpd-I], [(Por)Cmpd-II], and [(Por)Cmpd- II···(LuH$^+$)] complexes; figures of UV−vis, NMR, and EPR spectra; plots of pseudo-first-order rate constants; LC-MS and ESI-MS data (PDF)

■ AUTHOR INFORMATION

Corresponding Author

Gayan B. Wijeratne − *Department of Chemistry and O'Neal Comprehensive Cancer Center, University of Alabama at Birmingham, Birmingham, Alabama 35205, United States*; orcid.org/0000-0001-7609-6406; Email: wijeratne@uab.edu

Authors

Pritam Mondal − *Department of Chemistry and O'Neal Comprehensive Cancer Center, University of Alabama at Birmingham, Birmingham, Alabama 35205, United States*; orcid.org/0000-0002-7071-1970

Shanuk Rajapakse − *Department of Chemistry and O'Neal Comprehensive Cancer Center, University of Alabama at Birmingham, Birmingham, Alabama 35205, United States*; orcid.org/0000-0002-6001-8881

Complete contact information is available at: https://pubs.acs.org/10.1021/jacs.1c11068

Notes

The authors declare no competing financial interest.

■ ACKNOWLEDGMENTS

This work was supported by the U.S. National Science Foundation CAREER Award CHE-2045005 (to G.B.W.). G.B.W. also gratefully acknowledges The University of Alabama at Birmingham (UAB) for startup funds and the faculty development grant program (UAB-FDGP). Authors would like to thank Prof. Mary Ellen Zvanut (UAB), Dr. Ken Belmore (University of Alabama, Tuscaloosa (UA)), Dr. Qiaoli Liang (UA), and Landon Wilson (UAB) for assistance with EPR, ^{2}H NMR, and mass spectrometry/LC-MS experiments. Purchase of the AB Sciex 5600 TripleTOF mass spectrometer in the Targeted Metabolomics and Proteomics Laboratory (TMPL) at UAB came from funds provided by the NCRR grant: S10 RR027822-01. Funds for the operation of TMPL come in part from the UAB O'Brien Acute Kidney Injury Center (P30 DK079337).

■ REFERENCES

(1) Huang, X.; Groves, J. T. Beyond ferryl-mediated hydroxylation: 40 years of the rebound mechanism and C-H activation. *J. Biol. Inorg. Chem.* **2017**, *22*, 185.

(2) Adam, S. M.; Wijeratne, G. B.; Rogler, P. J.; Diaz, D. E.; Quist, D. A.; Liu, J. J.; Karlin, K. D. Synthetic Fe/Cu Complexes: Toward Understanding Heme-Copper Oxidase Structure and Function. *Chem. Rev.* **2018**, *118*, 10840.

(3) Sono, M.; Roach, M. P.; Coulter, E. D.; Dawson, J. H. Heme-Containing Oxygenases. *Chem. Rev.* **1996**, *96*, 2841.

(4) Meunier, B.; de Visser, S. P.; Shaik, S. Mechanism of Oxidation Reactions Catalyzed by Cytochrome P450 Enzymes. *Chem. Rev.* **2004**, *104*, 3947.

(5) Ortiz de Montellano, P. R. Hydrocarbon Hydroxylation by Cytochrome P450 Enzymes. *Chem. Rev.* **2010**, *110*, 932.

(6) Groves, J. T. High-valent iron in chemical and biological oxidations. *J. Inorg. Biochem.* **2006**, *100*, 434.

(7) Matsui, T.; Nakajima, A.; Fujii, H.; Matera, K. M.; Migita, C. T.; Yoshida, T.; Ikeda-Saito, M. O_2- and H_2O_2-dependent Verdoheme Degradation by Heme Oxygenase: Reaction Mechanisms and Potential Physiological Roles of the Dual Pathway Degradation. *J. Biol. Chem.* **2005**, *280*, 36833.

(8) Efimov, I.; Basran, J.; Thackray, S. J.; Handa, S.; Mowat, C. G.; Raven, E. L. Structure and Reaction Mechanism in the Heme Dioxygenases. *Biochemistry* **2011**, *50*, 2717.

(9) Vaillancourt, F. H.; Yeh, E.; Vosburg, D. A.; Garneau-Tsodikova, S.; Walsh, C. T. Nature's Inventory of Halogenation Catalysts: Oxidative Strategies Predominate. *Chem. Rev.* **2006**, *106*, 3364.

(10) Shaik, S.; de Visser, S. P.; Ogliaro, F.; Schwarz, H.; Schröder, D. Two-state reactivity mechanisms of hydroxylation and epoxidation by cytochrome P-450 revealed by theory. *Curr. Opin. Chem. Biol.* **2002**, *6*, 556.

(11) Huang, X.; Groves, J. T. Oxygen Activation and Radical Transformations in Heme Proteins and Metalloporphyrins. *Chem. Rev.* **2018**, *118*, 2491.

(12) Shin, I.; Wang, Y.; Liu, A. A new regime of heme-dependent aromatic oxygenase superfamily. *Proc. Nat. Acad. Sci.* **2021**, *118*, No. e2106561118.

(13) Wilks, A.; Ikeda-Saito, M. Heme Utilization by Pathogenic Bacteria: Not All Pathways Lead to Biliverdin. *Acc. Chem. Res.* **2014**, *47*, 2291.

(14) Ferrer-Sueta, G.; Campolo, N.; Trujillo, M.; Bartesaghi, S.; Carballal, S.; Romero, N.; Alvarez, B.; Radi, R. Biochemistry of Peroxynitrite and Protein Tyrosine Nitration. *Chem. Rev.* **2018**, *118*, 1338.

(15) Ye, Z.; Yue, L.; Shi, J.; Shao, M.; Wu, T. Role of IDO and TDO in Cancers and Related Diseases and the Therapeutic Implications. *J. Cancer* **2019**, *10*, 2771.

(16) Tracz, M. J.; Alam, J.; Nath, K. A. Physiology and Pathophysiology of Heme: Implications for Kidney Disease. *J. Am. Soc. Nephrol.* **2007**, *18*, 414.

(17) Matsuo, T.; Miyata, Y.; Mitsunari, K.; Yasuda, T.; Ohba, K.; Sakai, H. Pathological significance and prognostic implications of heme oxygenase 1 expression in non-muscle-invasive bladder cancer: Correlation with cell proliferation, angiogenesis, lymphangiogenesis and expression of VEGFs and COX-2. *Oncol. Lett.* **2017**, *13*, 275.

(18) Xie, K.; Fidler, I. J. Therapy of cancer metastasis by activation of the inducible nitric oxide synthase. *Cancer Metastasis Rev.* **1998**, *17*, 55.
(19) Ying, L.; Hofseth, A. B.; Browning, D. D.; Nagarkatti, M.; Nagarkatti, P. S.; Hofseth, L. J. Nitric Oxide Inactivates the Retinoblastoma Pathway in Chronic Inflammation. *Cancer Res.* **2007**, *67*, 9286.
(20) Baglia, R. A.; Zaragoza, J. P. T.; Goldberg, D. P. Biomimetic Reactivity of Oxygen-Derived Manganese and Iron Porphyrinoid Complexes. *Chem. Rev.* **2017**, *117*, 13320.
(21) Guo, M.; Corona, T.; Ray, K.; Nam, W. Heme and Nonheme High-Valent Iron and Manganese Oxo Cores in Biological and Abiological Oxidation Reactions. *ACS Cent. Sci.* **2019**, *5*, 13.
(22) Nam, W. High-Valent Iron(IV)-Oxo Complexes of Heme and Non-Heme Ligands in Oxygenation Reactions. *Acc. Chem. Res.* **2007**, *40*, 522.
(23) Fujii, H. Chapter 9 Model Complexes of Heme Peroxidases. In *Heme Peroxidases*; Raven, E., Dunford, B., Eds.; The Royal Society of Chemistry, 2016; p 181.
(24) Mukherjee, G.; Satpathy, J. K.; Bagha, U. K.; Mubarak, M. Q. E.; Sastri, C. V.; de Visser, S. P. Inspiration from Nature: Influence of Engineered Ligand Scaffolds and Auxiliary Factors on the Reactivity of Biomimetic Oxidants. *ACS Catal.* **2021**, *11*, 9761.
(25) van Deurzen, M. P. J.; van Rantwijk, F.; Sheldon, R. A. Synthesis of substituted oxindoles by chloroperoxidase catalyzed oxidation of indoles. *J. Mol. Catal. B: Enzym.* **1996**, *2*, 33.
(26) van de Velde, F.; van Rantwijk, F.; Sheldon, R. A. Selective oxidations with molecular oxygen, catalyzed by chloroperoxidase in the presence of a reductant. *J. Mol. Catal. B: Enzym.* **1999**, *6*, 453.
(27) Zhang, R.; He, Q.; Chatfield, D.; Wang, X. Paramagnetic Nuclear Magnetic Resonance Relaxation and Molecular Mechanics Studies of the Chloroperoxidase-Indole Complex: Insights into the Mechanism of Chloroperoxidase-Catalyzed Regioselective Oxidation of Indole. *Biochemistry* **2013**, *52*, 3688.
(28) Malewschik, T.; Ghiladi, R. A. Dehaloperoxidase: An enzymatic Swiss army knife. *Coord. Chem. Rev.* **2021**, *441*, 213976.
(29) Barrios, D. A.; D'Antonio, J.; McCombs, N. L.; Zhao, J.; Franzen, S.; Schmidt, A. C.; Sombers, L. A.; Ghiladi, R. A. Peroxygenase and Oxidase Activities of Dehaloperoxidase-Hemoglobin from Amphitrite ornata. *J. Am. Chem. Soc.* **2014**, *136*, 7914.
(30) Gillam, E. M. J.; Notley, L. M.; Cai, H.; De Voss, J. J.; Guengerich, F. P. Oxidation of Indole by Cytochrome P450 Enzymes. *Biochemistry* **2000**, *39*, 13817.
(31) Skordos, K. W.; Skiles, G. L.; Laycock, J. D.; Lanza, D. L.; Yost, G. S. Evidence Supporting the Formation of 2,3-Epoxy-3-methylindoline: A Reactive Intermediate of the Pneumotoxin 3-Methylindole. *Chem. Res. Toxicol.* **1998**, *11*, 741.
(32) Ling, K.-Q.; Sayre, L. M. Horseradish peroxidase-mediated aerobic and anaerobic oxidations of 3-alkylindoles. *Biorg. Med. Chem.* **2005**, *13*, 3543.
(33) Xu, J.; Shoji, O.; Fujishiro, T.; Ohki, T.; Ueno, T.; Watanabe, Y. Construction of biocatalysts using the myoglobin scaffold for the synthesis of indigo from indole. *Catal. Sci. Technol.* **2012**, *2*, 739.
(34) Kuo, H. H.; Mauk, A. G. Indole peroxygenase activity of indoleamine 2,3-dioxygenase. *Proc. Nat. Acad. Sci.* **2012**, *109*, 13966.
(35) Freewan, M.; Rees, M. D.; Plaza, T. S. S.; Glaros, E.; Lim, Y. J.; Wang, X. S.; Yeung, A. W. S.; Witting, P. K.; Terentis, A. C.; Thomas, S. R. Human Indoleamine 2,3-Dioxygenase Is a Catalyst of Physiological Heme Peroxidase Reactions: Implications for the Inhibition of Dioxygenase Activity by Hydrogen Peroxide. *J. Biol. Chem.* **2013**, *288*, 1548.
(36) Zhang, Y.; Zou, Y.; Brock, N. L.; Huang, T.; Lan, Y.; Wang, X.; Deng, Z.; Tang, Y.; Lin, S. Characterization of 2-Oxindole Forming Heme Enzyme MarE, Expanding the Functional Diversity of the Tryptophan Dioxygenase Superfamily. *J. Am. Chem. Soc.* **2017**, *139*, 11887.
(37) Nam, W.; Park, S.-E.; Lim, I. K.; Lim, M. H.; Hong, J.; Kim, J. First Direct Evidence for Stereospecific Olefin Epoxidation and Alkane Hydroxylation by an Oxoiron(IV) Porphyrin Complex. *J. Am. Chem. Soc.* **2003**, *125*, 14674.
(38) Moody, P. C. E.; Raven, E. L. The Nature and Reactivity of Ferryl Heme in Compounds I and II. *Acc. Chem. Res.* **2018**, *51*, 427.
(39) Sundaramoorthy, M.; Terner, J.; Poulos, T. L. The crystal structure of chloroperoxidase: a heme peroxidase-cytochrome P450 functional hybrid. *Structure* **1995**, *3*, 1367.
(40) Sugimoto, H.; Oda, S.-I.; Otsuki, T.; Hino, T.; Yoshida, T.; Shiro, Y. Crystal structure of human indoleamine 2,3-dioxygenase: Catalytic mechanism of O_2 incorporation by a heme-containing dioxygenase. *Proc. Natl. Acad. Sci. U. S. A.* **2006**, *103*, 2611.
(41) Yost, G. S. Mechanisms of 3-methylindole pneumotoxicity. *Chem. Res. Toxicol.* **1989**, *2*, 273.
(42) Weems, J. M.; Yost, G. S. 3-Methylindole Metabolites Induce Lung CYP1A1 and CYP2F1 Enzymes by AhR and Non-AhR Mechanisms, Respectively. *Chem. Res. Toxicol.* **2010**, *23*, 696.
(43) Weems, J. M.; Cutler, N. S.; Moore, C.; Nichols, W. K.; Martin, D.; Makin, E.; Lamb, J. G.; Yost, G. S. 3-Methylindole is Mutagenic and a Possible Pulmonary Carcinogen. *Toxicol. Sci.* **2009**, *112*, 59.
(44) Hornyák, L.; Dobos, N.; Koncz, G.; Karányi, Z.; Páll, D.; Szabó, Z.; Halmos, G.; Székvölgyi, L. The Role of Indoleamine-2,3-Dioxygenase in Cancer Development, Diagnostics, and Therapy. *Front. Immunol.* **2018**, *9*, 1.
(45) Coletti, A.; Greco, F. A.; Dolciami, D.; Camaioni, E.; Sardella, R.; Pallotta, M. T.; Volpi, C.; Orabona, C.; Grohmann, U.; Macchiarulo, A. Advances in indoleamine 2,3-dioxygenase 1 medicinal chemistry. *Med. Chem. Comm.* **2017**, *8*, 1378.
(46) Labadie, B. W.; Bao, R.; Luke, J. J. Reimagining IDO pathway inhibition in cancer immunotherapy via downstream focus on the tryptophan-kynurenine-aryl hydrocarbon axis. *Clin. Cancer. Res.* **2019**, *25*, 1462.
(47) Paul, S.; Roy, A.; Deka, S. J.; Panda, S.; Srivastava, G. N.; Trivedi, V.; Manna, D. Synthesis and evaluation of oxindoles as promising inhibitors of the immunosuppressive enzyme indoleamine 2,3-dioxygenase 1. *Med. Chem. Commun.* **2017**, *8*, 1640.
(48) Lewis-Ballester, A.; Forouhar, F.; Kim, S.-M.; Lew, S.; Wang, Y.; Karkashon, S.; Seetharaman, J.; Batabyal, D.; Chiang, B.-Y.; Hussain, M.; Correia, M. A.; Yeh, S.-R.; Tong, L. Molecular basis for catalysis and substrate-mediated cellular stabilization of human tryptophan 2,3-dioxygenase. *Sci. Rep.* **2016**, *6*, 35169.
(49) Efimov, I.; Basran, J.; Thackray, S. J.; Handa, S.; Mowat, C. G.; Raven, E. L.; Eldik, R. V.; Ivanović-Burmazović, I. Chapter 2 - Heme-containing Dioxygenases. *Adv. Inorg. Chem.* **2012**, *64*, 33−51.
(50) Raven, E. L. A short history of heme dioxygenases: rise, fall and rise again. *J. Biol. Inorg. Chem.* **2017**, *22*, 175.
(51) Kaur, M. Chapter 6 - Oxindole: A Nucleus Enriched With Multitargeting Potential Against Complex Disorders. In *Key Heterocycle Cores for Designing Multitargeting Molecules*; Silakari, O., Ed.; Elsevier, 2018; p 211.
(52) Kaur, M.; Singh, M.; Chadha, N.; Silakari, O. Oxindole: A chemical prism carrying plethora of therapeutic benefits. *Eur. J. Med. Chem.* **2016**, *123*, 858.
(53) Peddibhotla, S. 3-Substituted-3-hydroxy-2-oxindole, an Emerging New Scaffold for Drug Discovery with Potential Anti-Cancer and other Biological Activities. *Curr. Bioact. Compd.* **2009**, *5*, 20.
(54) Khetmalis, Y. M.; Shivani, M.; Murugesan, S.; Chandra Sekhar, K. V. G. Oxindole and its derivatives: A review on recent progress in biological activities. *Biomed. Pharmacother.* **2021**, *141*, 111842.
(55) Romagnoli, R.; Baraldi, P. G.; Prencipe, F.; Oliva, P.; Baraldi, S.; Salvador, M. K.; Lopez-Cara, L. C.; Bortolozzi, R.; Mattiuzzo, E.; Basso, G.; Viola, G. Design, synthesis and biological evaluation of 3-substituted-2-oxindole hybrid derivatives as novel anticancer agents. *Eur. J. Med. Chem.* **2017**, *134*, 258.
(56) Lv, K.; Wang, L.-L.; Zhou, X.-B.; Liu, M.-L.; Liu, H.-Y.; Zheng, Z.-B.; Li, S. Synthesis and in vitro antitumor activity of 1-(3-dimethylamino)propyl indolin-2-one derivatives. *Med. Chem. Res.* **2013**, *22*, 1723.
(57) Yasuda, D.; Takahashi, K.; Ohe, T.; Nakamura, S.; Mashino, T. Antioxidant activities of 5-hydroxyoxindole and its 3-hydroxy-3-

phenacyl derivatives: The suppression of lipid peroxidation and intracellular oxidative stress. *Biorg. Med. Chem.* **2013**, *21*, 7709.

(58) Rottmann, M.; McNamara, C.; Yeung, B. K. S.; Lee, M. C. S.; Zou, B.; Russell, B.; Seitz, P.; Plouffe, D. M.; Dharia, N. V.; Tan, J.; Cohen, S. B.; Spencer, K. R.; González-Páez, G. E.; Lakshminarayana, S. B.; Goh, A.; Suwanarusk, R.; Jegla, T.; Schmitt, E. K.; Beck, H.-P.; Brun, R.; Nosten, F.; Renia, L.; Dartois, V.; Keller, T. H.; Fidock, D. A.; Winzeler, E. A.; Diagana, T. T. Spiroindolones, a Potent Compound Class for the Treatment of Malaria. *Science* **2010**, *329*, 1175.

(59) Watanabe, H.; Ono, M.; Kimura, H.; Matsumura, K.; Yoshimura, M.; Okamoto, Y.; Ihara, M.; Takahashi, R.; Saji, H. Synthesis and biological evaluation of novel oxindole derivatives for imaging neurofibrillary tangles in Alzheimer's disease. *Bioorg. Med. Chem. Lett.* **2012**, *22*, 5700.

(60) Tokunaga, T.; Hume, W. E.; Nagamine, J.; Kawamura, T.; Taiji, M.; Nagata, R. Structure-activity relationships of the oxindole growth hormone secretagogues. *Bioorg. Med. Chem. Lett.* **2005**, *15*, 1789.

(61) Singh, H.; Sindhu, J.; Khurana, J. M.; Sharma, C.; Aneja, K. R. Ultrasound promoted one pot synthesis of novel fluorescent triazolyl spirocyclic oxindoles using DBU based task specific ionic liquids and their antimicrobial activity. *Eur. J. Med. Chem.* **2014**, *77*, 145.

(62) Ingrand, S.; Barrier, L.; Lafay-Chebassier, C.; Fauconneau, B.; Page, G.; Hugon, J. The oxindole/imidazole derivative C16 reduces in vivo brain PKR activation. *FEBS Lett.* **2007**, *581*, 4473.

(63) Paira, P.; Hazra, A.; Kumar, S.; Paira, R.; Sahu, K. B.; Naskar, S.; Saha, P.; Mondal, S.; Maity, A.; Banerjee, S.; Mondal, N. B. Efficient synthesis of 3,3-diheteroaromatic oxindole analogues and their in vitro evaluation for spermicidal potential. *Bioorg. Med. Chem. Lett.* **2009**, *19*, 4786.

(64) Guo, H.; Zhang, X.; Cui, Y.; Deng, W.; Xu, D.; Han, H.; Wang, H.; Chen, Y.; Li, Y.; Wu, D. Isorhynchophylline protects against pulmonary arterial hypertension and suppresses PASMCs proliferation. *Biochem. Biophys. Res. Commun.* **2014**, *450*, 729.

(65) Chowdhury, S.; Chafeev, M.; Liu, S.; Sun, J.; Raina, V.; Chui, R.; Young, W.; Kwan, R.; Fu, J.; Cadieux, J. A. Discovery of XEN907, a spirooxindole blocker of NaV1.7 for the treatment of pain. *Bioorg. Med. Chem. Lett.* **2011**, *21*, 3676.

(66) Roskoski, R. Sunitinib: A VEGF and PDGF receptor protein kinase and angiogenesis inhibitor. *Biochem. Biophys. Res. Commun.* **2007**, *356*, 323.

(67) Goodman, V. L.; Rock, E. P.; Dagher, R.; Ramchandani, R. P.; Abraham, S.; Gobburu, J. V. S.; Booth, B. P.; Verbois, S. L.; Morse, D. E.; Liang, C. Y.; Chidambaram, N.; Jiang, J. X.; Tang, S.; Mahjoob, K.; Justice, R.; Pazdur, R. Approval Summary: Sunitinib for the Treatment of Imatinib Refractory or Intolerant Gastrointestinal Stromal Tumors and Advanced Renal Cell Carcinoma. *Clin. Cancer. Res.* **2007**, *13*, 1367.

(68) London, C. A.; Malpas, P. B.; Wood-Follis, S. L.; Boucher, J. F.; Rusk, A. W.; Rosenberg, M. P.; Henry, C. J.; Mitchener, K. L.; Klein, M. K.; Hintermeister, J. G.; Bergman, P. J.; Couto, G. C.; Mauldin, G. N.; Michels, G. M. Multi-center, Placebo-controlled, Double-blind, Randomized Study of Oral Toceranib Phosphate (SU11654), a Receptor Tyrosine Kinase Inhibitor, for the Treatment of Dogs with Recurrent (Either Local or Distant) Mast Cell Tumor Following Surgical Excision. *Clin. Cancer. Res.* **2009**, *15*, 3856.

(69) Kauffman, R. F.; Robertson, D. W.; Franklin, R. B.; Sandusky, G. E., Jr; Dies, F.; McNay, J. L.; Hayes, J. S. Indolidan: A Potent, Long-Acting Cardiotonic and Inhibitor of Type IV Cyclic AMP Phosphodiesterase. *Cardiovasc. Drug Rev.* **1990**, *8*, 303.

(70) Bethke, T.; Brunkhorst, D.; der Leyen, H. V.; Meyer, W.; Nigbur, R.; Scholz, H. Mechanism of action and cardiotonic activity of a new phosphodiesterase inhibitor, the benzimidazole derivative adibendan (BM 14.478), in guinea-pig hearts. *Naunyn-Schmiedeberg's Arch. Pharmacol.* **1988**, *337*, 576.

(71) Mukherjee, M.; Dey, A. Rejigging Electron and Proton Transfer to Transition between Dioxygenase, Monooxygenase, Peroxygenase, and Oxygen Reduction Activity: Insights from Bioinspired Constructs of Heme Enzymes. *JACS Au* **2021**, *1*, 1296.

(72) Mondal, P.; Wijeratne, G. B. Modeling Tryptophan/Indoleamine 2,3-Dioxygenase with Heme Superoxide Mimics: Is Ferryl the Key Intermediate? *J. Am. Chem. Soc.* **2020**, *142*, 1846.

(73) Mukherjee, M.; Dey, A. Catalytic C-H Bond Oxidation Using Dioxygen by Analogues of Heme Superoxide. *Inorg. Chem.* **2020**, *59*, 7415.

(74) Sacramento, J. J. D.; Goldberg, D. P. Oxidation of an indole substrate by porphyrin iron(iii) superoxide: relevance to indoleamine and tryptophan 2,3-dioxygenases. *Chem. Commun.* **2020**, *56*, 3089.

(75) Linhares, M.; Rebelo, S. L. H.; Simões, M. M. Q.; Silva, A. M. S.; Neves, M. G. P. M. S.; Cavaleiro, J. A. S.; Freire, C. Biomimetic oxidation of indole by Mn(III)porphyrins. *Applied Catalysis A: General* **2014**, *470*, 427.

(76) Rebelo, S. L. H.; Linhares, M.; Simões, M. M. Q.; Silva, A. M. S.; Neves, M. G. P. M. S.; Cavaleiro, J. A. S.; Freire, C. Indigo dye production by enzymatic mimicking based on an iron(III)porphyrin. *J. Catal.* **2014**, *315*, 33.

(77) Jiang, X.; Zheng, C.; Lei, L.; Lin, K.; Yu, C. Synthesis of 2-Oxindoles from Substituted Indoles by Hypervalent-Iodine Oxidation. *Eur. J. Org. Chem.* **2018**, *2018*, 1437.

(78) Zhao, G.; Liang, L.; Wang, E.; Lou, S.; Qi, R.; Tong, R. Fenton chemistry enables the catalytic oxidative rearrangement of indoles using hydrogen peroxide. *Green Chem.* **2021**, *23*, 2300.

(79) Xu, J.; Liang, L.; Zheng, H.; Chi, Y. R.; Tong, R. Green oxidation of indoles using halide catalysis. *Nat. Commun.* **2019**, *10*, 4754.

(80) Visser, S. P. Second-Coordination Sphere Effects on Selectivity and Specificity of Heme and Nonheme Iron Enzymes. *Chem. Eur. J.* **2020**, *26*, 5308.

(81) Ehudin, M. A.; Senft, L.; Franke, A.; Ivanović-Burmazović, I.; Karlin, K. D. Formation and Reactivity of New Isoporphyrins: Implications for Understanding the Tyr-His Cross-Link Cofactor Biogenesis in Cytochrome c Oxidase. *J. Am. Chem. Soc.* **2019**, *141*, 10632.

(82) Ehudin, M. A.; Gee, L. B.; Sabuncu, S.; Braun, A.; Moënne-Loccoz, P.; Hedman, B.; Hodgson, K. O.; Solomon, E. I.; Karlin, K. D. Tuning the Geometric and Electronic Structure of Synthetic High-Valent Heme Iron(IV)-Oxo Models in the Presence of a Lewis Acid and Various Axial Ligands. *J. Am. Chem. Soc.* **2019**, *141*, 5942.

(83) Ishimizu, Y.; Ma, Z.; Hada, M.; Fujii, H. Experimental and theoretical studies of the porphyrin ligand effect on the electronic structure and reactivity of oxoiron(iv) porphyrin π-cation-radical complexes. *J. Biol. Inorg. Chem.* **2019**, *24*, 483.

(84) Takahashi, A.; Yamaki, D.; Ikemura, K.; Kurahashi, T.; Ogura, T.; Hada, M.; Fujii, H. Effect of the Axial Ligand on the Reactivity of the Oxoiron(IV) Porphyrin π-Cation Radical Complex: Higher Stabilization of the Product State Relative to the Reactant State. *Inorg. Chem.* **2012**, *51*, 7296.

(85) Ehudin, M. A.; Quist, D. A.; Karlin, K. D. Enhanced Rates of C-H Bond Cleavage by a Hydrogen-Bonded Synthetic Heme High-Valent Iron(IV) Oxo Complex. *J. Am. Chem. Soc.* **2019**, *141*, 12558.

(86) Coordinating solvents, in this case THF, is required to cleanly generate Cmpd-II, which is in-line with previous reports (see reference 82). However, it has been previously shown that coordinating solvents do not impart strong axial ligand effects on the heme center of Cmpd-II. Ferric heme centers on the contrary, can more readily bind to coordinating solvents such as THF.

(87) Jennings, P.; Jones, A. C.; Mount, A. R.; Thomson, A. D. Electrooxidation of 5-substituted indoles. *J. Chem. Soc., Faraday Trans.* **1997**, *93*, 3791.

(88) Rangappa, K. S.; Ramachandra, H.; Mahadevappa, D. S.; Gowda, N. M. M. Osmium (VIII) catalyzed kinetics and mechanism of indoles oxidation with Aryl-N-haloamines in alkaline medium. *Int. J. Chem. Kinet.* **1996**, *28*, 265.

(89) Rangappa, K. S.; Esterline, D. T.; Mythily, C. K.; Mahadevappa, D. S.; Ambekar, S. Y. Oxidation of indoles by n-chloro-n-sodio-p-toluenesulphonamide in alkaline medium catalysed by osmium(VIII): a kinetic study. *Polyhedron* **1993**, *12*, 1719.

https://doi.org/10.1021/jacs.1c11068
J. Am. Chem. Soc. XXXX, XXX, XXX−XXX

(90) Kungumathilagam, D.; Karunakaran, K. Kinetics and mechanism of meso-tetraphenylporphyriniron(III) chloride (TPP) catalysed oxidation of indole by sodium perborate. *Polym. J. Chem. Technol.* **2013**, *15*, 107.
(91) Berglund, G. I.; Carlsson, G. H.; Smith, A. T.; Szöke, H.; Henriksen, A.; Hajdu, J. The catalytic pathway of horseradish peroxidase at high resolution. *Nature* **2002**, *417*, 463.
(92) The observed 80% incorporation of the ^{18}O-label in the oxindole products is most likely due to incomplete ^{18}O exchange between iodosylbenzene and $H_2{}^{18}O$. This could, among other reasons be due to (1) extremely insoluble nature of PhIO; (2) impaired stability of the Cmpd-I oxidant in the presence of $H_2{}^{18}O$ (a proton source); and (3) impaired stability of iodosylbenzene during sonication. Importantly, previous studies have also reported similar ^{18}O-label incorporation yields (~85%) when following this labeling method (see Nam, W.; Lim, M. H.; Oh, S. Y. *Inorg. Chem.* **2000**, *39*, 5572−5575. Goh, Y. M.; Nam, W. *Inorg. Chem.* 1999, *38*, 914−920). Using prolonged sonication times for the ^{18}O exchange reaction between iodosylbenzene and $H_2{}^{18}O$ decreased the ^{18}O incorporation in the oxindole products (Figure S16).
(93) Zhang, X.; Foote, C. S. Dimethyldioxirane oxidation of indole derivatives. Formation of novel indole-2,3-epoxides and a versatile synthetic route to indolinones and indolines. *J. Am. Chem. Soc.* **1993**, *115*, 8867.
(94) Unreacted starting material was recoverable for each indole substrate indicating the absence of any significant side reactions or byproduct formation. When excess oxidant was used, indole substrates were observed to undergo overoxidation preventing the formation of 2-oxindole products.
(95) While the exact reasonings governing the exclusive formation of 2-oxindole (but not 3-oxindole) are yet to be fully understood, we note that the sequence of mechanistic events warranted for these various products is different, which may lead to divergent overall favorabilities. Notably, previous work strongly suggests that accessing 3-oxindole could be a difficult task compared to 2-oxindole due to the high propensity of the former to undergo autoxidation: see Russell, G. A.; Kaupp, G. *J. Am. Chem. Soc.* **1969**, *91*, 3851.
(96) Nishikawa, K.; Honda, Y.; Fujii, H. Spectroscopic Evidence for Acid-Catalyzed Disproportionation Reaction of Oxoiron(IV) Porphyrin to Oxoiron(IV) Porphyrin π-Cation Radical and Iron(III) Porphyrin. *J. Am. Chem. Soc.* **2020**, *142*, 4980.
(97) A similar ρ value ($\rho = -1.0$) has been observed in a previous indole monooxygenation study involving an OsO_4 catalyst, where an analogous indole nucleophilic attack on the metal oxidant was found to be rate-limiting.
(98) Armarego, W. L. F.; Chai, C. Chapter 4 - Purification of Organic Chemicals. *Purification of Laboratory Chemicals*, Sixth ed.; Butterworth-Heinemann: Oxford, UK, 2009; p 88.
(99) Ghiladi, R. A.; Kretzer, R. M.; Guzei, I.; Rheingold, A. L.; Neuhold, Y.-M.; Hatwell, K. R.; Zuberbühler, A. D.; Karlin, K. D. $(F_8TPP)Fe^{II}/O_2$ Reactivity Studies {F_8TPP = Tetrakis(2,6-difluorophenyl)porphyrinate(2-)}: Spectroscopic (UV-Visible and NMR) and Kinetic Study of Solvent-Dependent (Fe/O_2 = 1:1 or 2:1) Reversible O_2-Reduction and Ferryl Formation. *Inorg. Chem.* **2001**, *40*, 5754.
(100) Hyun, M. Y.; Jo, Y. D.; Lee, J. H.; Lee, H. G.; Park, H. M.; Hwang, I. H.; Kim, K. B.; Lee, S. J.; Kim, C. Remarkable Solvent, Porphyrin Ligand, and Substrate Effects on Participation of Multiple Active Oxidants in Manganese(III) Porphyrin Catalyzed Oxidation Reactions. *Chem. Eur. J.* **2013**, *19*, 1810.
(101) Song, X.; Xu, C.; Du, D.; Zhao, Z.; Zhu, D.; Wang, M. Ring-Opening Diarylation of Siloxydifluorocyclopropanes by Ag(I) Catalysis: Stereoselective Construction of 2-Fluoroallylic Scaffold. *Org. Lett.* **2017**, *19*, 6542.
(102) Cooper, L.; Alonso, J. M.; Eagling, L.; Newson, H.; Herath, S.; Thomson, C.; Lister, A.; Howsham, C.; Cox, B.; Muñoz, M. P. Synthesis of a Novel Type of 2,3′-BIMs via Platinum-Catalysed Reaction of Indolylallenes with Indoles. *Chem. Eur. J.* **2018**, *24*, 6105.
(103) Cong, T.; Wang, H.; Li, X.; Wu, H.-H.; Zhang, J. Chiral bifunctional bisphosphine enabled enantioselective tandem Michael addition of tryptamine-derived oxindoles to ynones. *Chem. Commun.* **2019**, *55*, 9176.
(104) Curley, J. J.; Bergman, R. G.; Tilley, T. D. Preparation and physical properties of early-late heterobimetallic compounds featuring Ir-M bonds (M = Ti, Zr, Hf). *Dalton Trans.* **2012**, *41*, 192.
(105) Wang, J.; Schopfer, M. P.; Puiu, S. C.; Sarjeant, A. A. N.; Karlin, K. D. Reductive Coupling of Nitrogen Monoxide (•NO) Facilitated by Heme/Copper Complexes. *Inorg. Chem.* **2010**, *49*, 1404.
(106) Kang, M.-J.; Song, W. J.; Han, A.-R.; Choi, Y. S.; Jang, H. G.; Nam, W. Mechanistic Insight into the Aromatic Hydroxylation by High-Valent Iron(IV)-oxo Porphyrin π-Cation Radical Complexes. *J. Org. Chem.* **2007**, *72*, 6301.

https://doi.org/10.1021/jacs.1c11068
J. Am. Chem. Soc. XXXX, XXX, XXX−XXX